

EVOLUTION AND DISTRIBUTION OF CURRENT HELICITY IN FULL-SUN SIMULATIONS

A. R. YEATES AND D. H. MACKAY

School of Mathematics and Statistics, University of St. Andrews, St. Andrews KY16 9SS, UK; anthony@mcs.st-and.ac.uk, duncan@mcs.st-and.ac.uk

AND

A. A. VAN BALLEGOOIJEN

Harvard-Smithsonian Center for Astrophysics, 60 Garden Street, Cambridge, MA 02138; vanballe@cfa.harvard.edu

Received 2008 April 30; accepted 2008 May 13; 2008 June 3

ABSTRACT

Current helicity quantifies the location of twisted and sheared nonpotential structures in a magnetic field. We simulate the evolution of magnetic fields in the solar atmosphere in response to flux emergence and shearing by photospheric motions. In our global-scale simulation over many solar rotations, the latitudinal distribution of current helicity develops a clear statistical pattern, matching the observed hemispheric sign at active latitudes. In agreement with observations, there is significant scatter and intermixing of both signs of helicity, where we find local values of current helicity density that are much higher than those predicted by linear force-free extrapolations. Forthcoming full-disk vector magnetograms from the *Solar Dynamics Observatory* will provide an ideal opportunity to test our theoretical results on the evolution and distribution of current helicity, both globally and in single active regions.

Subject headings: Sun: activity — Sun: magnetic fields

1. INTRODUCTION

The twist of the solar magnetic field plays an important role in transient phenomena such as solar flares and coronal mass ejections, and in the dynamo processes that cause the 11 yr solar activity cycle. The magnetic twist can be measured in various ways. Magnetic helicity is an integral that quantifies the topological complexity of field lines, such as linking, twist, or kinking (Berger 1998, 1999). For a closed magnetic system, it is defined by $H_m = \int \mathbf{A} \cdot \mathbf{B} d^3x$, and alternative definitions have been developed for open systems (Berger & Field 1984; Finn & Antonsen 1985).

In this Letter we consider current helicity, which we define as

$$\alpha = \frac{\mathbf{j} \cdot \mathbf{B}}{B^2}, \quad (1)$$

where \mathbf{B} is the magnetic field and $\mathbf{j} = \nabla \times \mathbf{B}$ is the current density. The quantity α has the advantage that it describes the *local* distribution of twist and shear in the magnetic field, and that it is more readily determined from limited observational data than H_m , which requires global information. For a force-free field ($\mathbf{j} \times \mathbf{B} = 0$), we have $\mathbf{j} = \alpha \mathbf{B}$; here α , which may be a function of space, is a fundamental parameter that describes the torsion of the field lines around one another. Note that we shall not consider the *integral* current helicity $H_c = \int \mathbf{j} \cdot \mathbf{B} d^3x$, because, unlike H_m , it is not a near-conserved quantity in MHD (Démoulin 2007), and, in general, it does not even take the same sign as H_m (except for linear force-free fields where α is constant in space and α , H_c , and H_m all have the same sign; Hagyard & Pevtsov 1999).

There are two main techniques for estimating α from observed vector magnetograms, which so far only cover a small region of the solar surface, such as a single active region:

1. Compute $j_z = \partial B_y / \partial x - \partial B_x / \partial y$ and hence $\alpha_z = j_z / B_z$, which should give α exactly for a force-free field (Abramenko et al. 1996; Bao & Zhang 1998).

2. Compute a linear force-free extrapolation from B_z and choose the overall value, α_{best} , that best reproduces the ob-

served (B_x, B_y) -distribution over the region (Pevtsov et al. 1995; Longcope et al. 1998; Zhang 2006).

The studies by Hagino & Sakurai (2004) and Burnette et al. (2004) show that both techniques are generally consistent. The key result of these observations is a robust hemispheric rule whereby the average α -value is negative in the northern hemisphere and positive in the southern hemisphere, although there is significant scatter, including a mixture of signs of α within single active regions. This hemispheric pattern in α has also been found by Pevtsov et al. (2001), who reconstructed the radial and toroidal components of the global magnetic field under simplifying assumptions.

A transequatorial sign change in helicity is supported by numerous proxy observations, such as H α images of active region structure (Hale 1927), in situ heliospheric measurements (Smith & Bieber 1993), differential rotation (Berger & Ruzmaikin 2000), and filament/prominence magnetic fields (Rust 1967; Martin et al. 1994). Using newly developed simulations of the global coronal evolution, we have recently been able to reproduce the filament hemispheric pattern, including exceptions (with 96% agreement), in a comparison with 109 observed filaments (Yeates et al. 2007, 2008). In this Letter we describe the distribution of current helicity in a 30 month simulation, which we hope to compare with new magnetic observations from the NASA *Solar Dynamics Observatory* (SDO) mission.

2. CORONAL MODEL

Our simulations of the three-dimensional (3D) coronal field evolution (Yeates et al. 2008) use the coupled flux transport and magnetofrictional model of van Ballegoijen et al. (2000) in a domain extending from 0° to 360° in longitude, -80° to 80° in latitude, and R_\odot to $2.5 R_\odot$ in radius. The coronal magnetic field $\mathbf{B} = \nabla \times \mathbf{A}$ evolves *via* the nonideal induction equation

$$\frac{\partial \mathbf{A}}{\partial t} = \mathbf{v} \times \mathbf{B} - \eta_c \mathbf{j}, \quad (2)$$

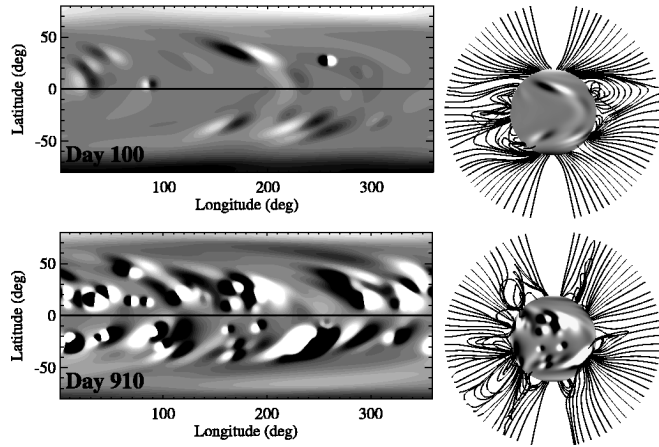


FIG. 1.—Simulated magnetic field on days 100 (*top*) and 910 (*bottom*). The left column shows the radial magnetic field on the solar surface (white for positive, black for negative), and the right column shows selected field lines of the 3D coronal magnetic field.

in response to flux emergence and advection by large-scale motions on the photospheric boundary. Rather than solve the full MHD system, we approximate the momentum equation by the magnetofrictional method (Yang et al. 1986), setting

$$\mathbf{v} = \frac{1}{\nu} \frac{\mathbf{j} \times \mathbf{B}}{B^2} + v_{\text{out}}(r) \hat{\mathbf{r}}. \quad (3)$$

This artificial velocity ensures evolution through a sequence of near force-free states. The second term is a radial outflow only imposed near the upper boundary, where it simulates the effect of the solar wind in opening up field lines in the radial direction (Mackay & van Ballegoijen 2006). The diffusivity η_c consists of a uniform background term and an enhancement in regions of strong current density \mathbf{j} (see Mackay & van Ballegoijen 2006).

The photospheric boundary conditions are described in Yeates et al. (2007); the surface flux transport model includes newly emerging magnetic bipoles based on active regions observed in synoptic normal-component magnetograms from the National Solar Observatory (NSO) at Kitt Peak. The emerging bipoles take a simple mathematical form, with properties chosen to match the location, size, tilt, and magnetic flux of the observed regions. They are inserted in 3D with a nonzero twist (magnetic helicity), chosen to match the observed sign of helicity in each hemisphere. The simulation illustrated in this Letter models 30 months of continuous evolution during the rising phase of Cycle 23 (from 1997 April 9 to 1999 October 10; Carrington rotations CR 1921–1954). From an initial potential field extrapolation, the photospheric and coronal fields were evolved forward continuously for 914 days, with 396 new bipoles inserted during this time. Two example snapshots of the simulated magnetic field are shown in Figure 1.

3. SOURCES OF HELICITY IN SINGLE ACTIVE REGIONS

To illustrate the sources of current helicity in our simulation within an individual active region, Figure 2 zooms in to a bipole in the northern hemisphere that emerged on day 136 (as measured from the start of the simulation).

There are three main sources of coronal currents and helicity in our model:

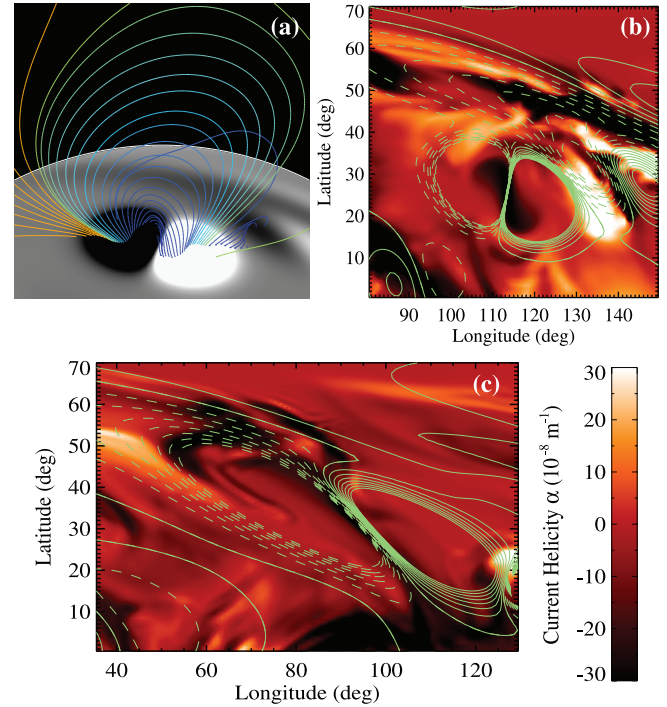


FIG. 2.—Structure of a single bipolar region, showing (a) magnetic field structure, (b) distribution of current helicity α on day 140, and (c) distribution of α on day 190. In (a), the gray shading shows radial magnetic field strength on the solar surface (black negative, white positive), and the colored lines show selected coronal field lines. In (b) and (c), the contours of α at height 14 Mm are shown in the color scale, and the green contours show the strength of the radial surface magnetic field (solid for positive, dashed for negative).

1. The new bipoles emerge twisted. This twist is initially concentrated down toward the center of the bipole, as seen from the field lines in Figure 2a that are skewed as they cross the bipole’s central polarity inversion line (PIL). The sigmoidal concentration of negative α at the center of the bipole is clearly seen on day 140 in Figure 2b.

2. When the bipoles emerge, they displace older fields and produce currents at the interface between old and new flux systems (see Yeates et al. 2008). In Figure 2b, this is visible at the northwest edge of the new bipole, where it adjoins a preexisting bipole and a layer of positive α has developed. Note that this is opposite in sign to that from the twist of the new region, as seen in Figure 2a. This corresponds to field lines that are oppositely skewed at this edge of the new bipole, as compared to those across the central PIL. This is just one example of how both signs of α may naturally be produced within a single active region, as found in observations.

3. Over time, surface motions shear the coronal field, generating further currents. This is visible in Figure 2c, which shows the distribution of α for the same region on day 190, after 50 days evolution. There is a significant buildup of negative α , particularly at the north and south ends of the bipole where helicity was initially low. This buildup is caused by differential rotation and convergence (due to supergranular diffusion).

In addition to these sources of current helicity, it may also be locally reduced by diffusive cancellation and reconnection. Also, helicity is periodically removed through the top boundary of the domain when excessive buildup of twist leads to local-

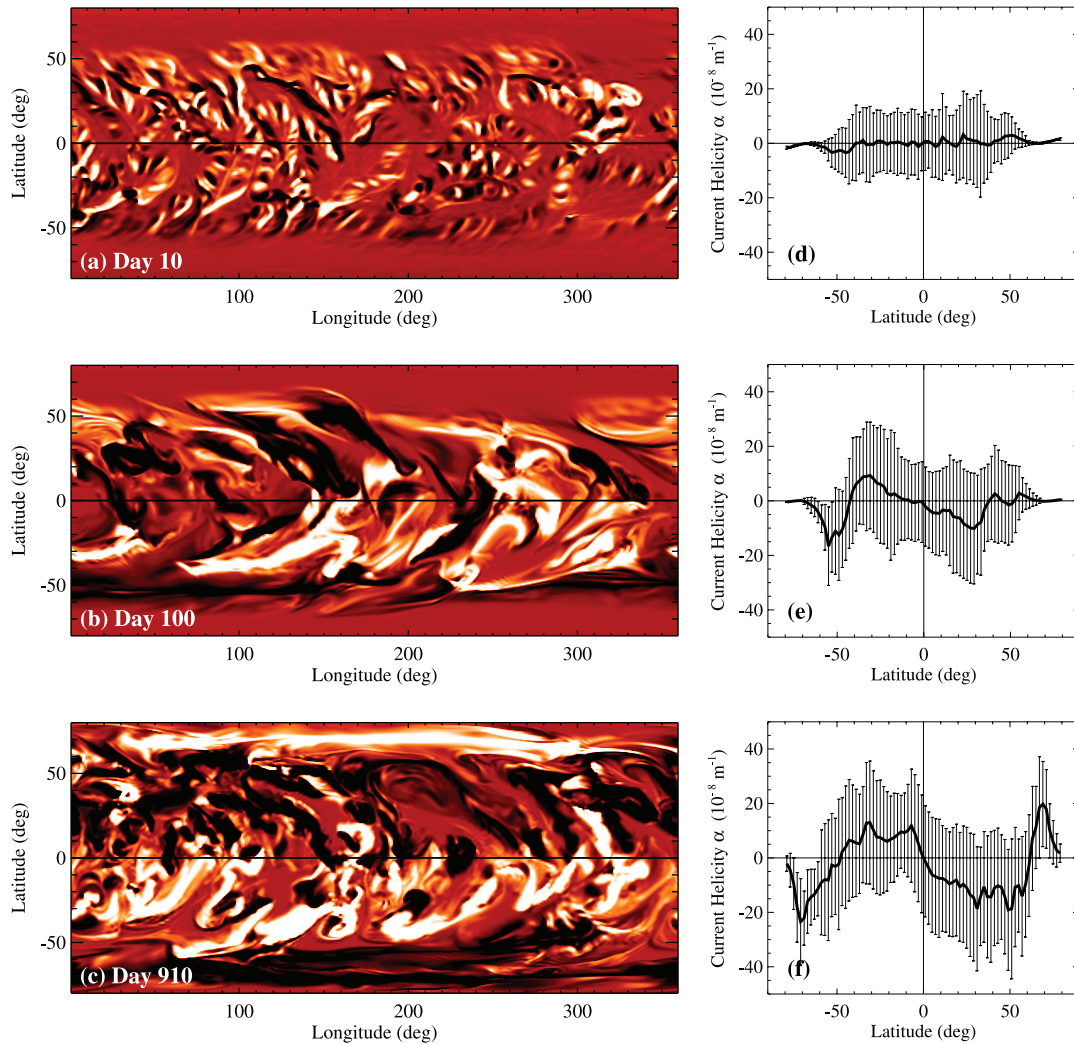


FIG. 3.—Global distribution of α at height 14 Mm on days 10, 100, and 910. The left column shows contours of α (white for positive and black for negative, saturation level $\pm 20 \times 10^{-8} \text{ m}^{-1}$). The right column shows the latitudinal profile, averaged over longitude in 2° latitude bins. Error bars show 1σ .

ized temporary losses of equilibrium and the ejection of twisted flux ropes (Mackay & van Ballegoijen 2006).

4. GLOBAL DISTRIBUTION OF CURRENT HELICITY

The global distribution of current helicity, α , is shown in Figure 3 at days 10, 100, and 910 of the simulation. From the initial potential field on day 0 (with $\alpha = 0$ everywhere), a pattern of intermixed positive and negative α has developed by day 10 that is simply due to photospheric shearing—this is before the first active region emergence. After about 100 days, a clear latitudinal trend in α emerges, although there is still significant local variation in both strength and sign. This pattern persists for the rest of the simulation, and up to medium heights in the 3D corona (nearer the top of the computational box, high values of α become localized to closed field regions, with $\alpha \approx 0$ where the field is open).

In Figures 3d, 3e, and 3f, it can be seen how the mean α at low latitudes (0° to about 50°) develops into the observed hemispheric trend, although with considerable scatter, as observed on the real Sun. However, at high latitudes, the sign of α is reversed. These polar reversals correspond to the east-west PILs at the polar crown boundaries and move steadily poleward through the simulation as the polar crowns reduce in size to-

ward polar field reversal (we are approaching solar maximum). This opposite sign of α is caused by differential rotation of the predominantly north-south field lines at this latitude and is a well-documented problem for theoretical models (van Ballegoijen & Martens 1990; Rust & Kumar 1994). At lower latitudes, as was illustrated by Figure 2c, differential rotation of north-south PILs produces the observed hemispheric sign of helicity (Zirker et al. 1997).

Figure 3 shows mean values of α at active latitudes of the order 10^{-7} m^{-1} . The actual maximum and minimum values recorded on day 910 of the simulation were 2.24×10^{-6} and $-1.84 \times 10^{-6} \text{ m}^{-1}$, respectively. A key result of this study is that these values are much higher than those estimated from linear force-free extrapolations. Such solutions suffer a constraint on the maximum α in order to obtain a decay with height (Aulanier & Démoulin 1998), requiring that $\alpha < 2\pi/L_x$ (the “first resonant value”), where L_x is the horizontal length of the periodic box. The linear force-free model of an observed filament by Aulanier et al. (2000) has $\alpha = 2.3 \times 10^{-8} \text{ m}^{-1}$, and for the solutions of Mackay et al. (1999), this first resonant value was at $\alpha = 4.24 \times 10^{-8} \text{ m}^{-1}$. By contrast, studies using nonlinear force-free extrapolations from vector magnetograms using the Grad-Rubin-type method (Amari et al. 1997) find locally higher

values of α (e.g., Bleybel et al. 2002). They are also more realistic because they allow variable α within a single region, as in our simulations. For a particular active region, Régnier et al. (2002) found maximum values of the order 10^{-6} m^{-1} , consistent with the results of our simulations.

5. DISCUSSION

In this Letter we have shown how our 3D simulations of the global coronal magnetic field evolution are able to model the development and transport of current helicity, α , over many solar rotations. We find a clear latitudinal pattern of α that persists throughout the simulation, although, locally within single bipoles, there is significant scatter and intermixing of both signs of α , in agreement with observations. Local values may be much higher than those predicted by linear force-free extrapolations.

With existing measurements of α limited to vector magnetograms of individual active regions, robust observations of the latitudinal distribution of α await full-disk vector magnetograms. These will shortly be available from the *SDO* satellite. In particular, the Helioseismic and Magnetic Imager will provide synoptic full-disk vector magnetograms at $1''$ resolution and approximately 90 s cadence. This will offer an exciting opportunity to test and refine our theoretical model for the coronal magnetic field. In particular, consistent measurements over a large portion of the solar cycle will allow us to consider how the helicity distribution varies over both space and time.

Whether there is a systematic variation in the latitudinal trend of helicity over the solar cycle remains an unresolved issue (Sokoloff et al. 2006; Pevtsov et al. 2008) that has implications

for the subsurface origin of helicity (Choudhuri et al. 2004). Indeed, Kleeorin et al. (2003) showed that observations of α in active regions provide important constraints on theories of the solar dynamo itself (see also Sokoloff 2007). Ejection of helical fields from the corona, as included in our simulations, is also thought to play an important role in sustaining the solar cycle (Blackman & Brandenburg 2003).

A particular feature of our results is the sign reversal of current helicity at the high-latitude polar crowns. This would appear to be in conflict with observations of magnetic fields in polar crown filaments, which show no such reversal in their chirality pattern (Rust 1967; Leroy et al. 1983; Martin et al. 1994). We hope to address this outstanding issue in longer simulations covering a greater portion of the solar cycle. It is not at present clear whether longer term poleward transport of the correct sign of helicity will be enough to counteract the effect of differential rotation on the north-south-oriented field lines at these latitudes. Observations of vector magnetic fields in the polar regions, such as those being made by *Hinode* (Lites et al. 2008) and those soon to be made by the *SDO* mission, should help to constrain our models.

Financial support for A. R. Y. and D. H. M. was provided by the UK STFC. D. H. M. and A. A. v. B. would also like to thank the ISSI in Bern for support. The simulations were performed on the UKMHD parallel computer at St. Andrews, funded jointly by SRIF/STFC. Synoptic magnetogram data from NSO/Kitt Peak was produced cooperatively by NSF/NOAO, NASA/GSFC, and NOAA/SEL and made publicly accessible on the World Wide Web.

REFERENCES

- Abramenko, V. I., Wang, T., & Yurchishin, V. B. 1996, *Sol. Phys.*, 168, 75
 Amari, T., Aly, J. J., Luciani, J. F., & Boulmezaoud, T. Z. 1997, *Sol. Phys.*, 174, 129
 Aulanier, G., & Démoulin, P. 1998, *A&A*, 329, 1125
 Aulanier, G., Srivastava, N., & Martin, S. F. 2000, *ApJ*, 543, 447
 Bao, S., & Zhang, H. 1998, *ApJ*, 496, L43
 Berger, M. A. 1998, in *IAU Colloq. 167, New Perspectives on Solar Prominences*, ed. D. Webb, D. Rust, & B. Schmieder (ASP Conf. Ser. 150; San Francisco: ASP), 102
 ———. 1999, *Plasma Phys. Controlled Fusion*, 41, B167
 Berger, M. A., & Field, G. B. 1984, *J. Fluid Mech.*, 147, 133
 Berger, M. A., & Ruzmaikin, A. 2000, *J. Geophys. Res.*, 105, 10481
 Blackman, E. G., & Brandenburg, A. 2003, *ApJ*, 584, L99
 Bleybel, A., Amari, T., van Driel-Gesztelyi, L., & Leka, K. D. 2002, *A&A*, 395, 685
 Burnette, A. B., Canfield, R. C., & Pevtsov, A. A. 2004, *ApJ*, 606, 565
 Choudhuri, A. R., Chatterjee, P., & Nandy, D. 2004, *ApJ*, 615, L57
 Démoulin, P. 2007, *Adv. Space Res.*, 39, 1674
 Finn, J. H., & Antonsen, T. M. 1985, *Comments Plasma Phys. Controlled Fusion*, 9, 111
 Hagino, M., & Sakurai, T. 2004, *PASJ*, 56, 831
 Hagyard, M. J., & Pevtsov, A. A. 1999, *Sol. Phys.*, 189, 25
 Hale, G. E. 1927, *Nature*, 119, 708
 Kleeorin, N., Kuzanyan, K., Moss, D., Rogachevskii, I., Sokoloff, D., & Zhang, H. 2003, *A&A*, 409, 1097
 Leroy, J.-L., Bommier, V., & Sahal-Brechot, S. 1983, *Sol. Phys.*, 83, 135
 Lites, B. W., et al. 2008, *ApJ*, 672, 1237
 Longcope, D. W., Fisher, G. H., & Pevtsov, A. A. 1998, *ApJ*, 507, 417
 Mackay, D. H., Longbottom, A. W., & Priest, E. R. 1999, *Sol. Phys.*, 185, 87
 Mackay, D. H. & van Ballegoijen, A. A. 2006, *ApJ*, 641, 577
 Martin, S. F., Bilimoria, R., & Tracadas, P. W. 1994, in *Solar Surface Magnetism*, ed. R. J. Rutten & C. J. Schrijver (New York: Springer), 303
 Pevtsov, A. A., Canfield, R. C., & Latushko, S. M. 2001, *ApJ*, 549, L261
 Pevtsov, A. A., Canfield, R. C., & Metcalf, T. R. 1995, *ApJ*, 440, L109
 Pevtsov, A. A., Canfield, R. C., Sakurai, T., & Hagino, M. 2008, *ApJ*, 677, 719
 Régnier, S., Amari, T., & Kersalé, E. 2002, *A&A*, 392, 1119
 Rust, D. M. 1967, *ApJ*, 150, 313
 Rust, D. M. & Kumar, A. 1994, *Sol. Phys.*, 155, 69
 Smith, C. W., & Bieber, J. W. 1993, *Proc. 23rd Int. Cosmic-Ray Conf. (Calgary)*, 493
 Sokoloff, D. 2007, *Plasma Phys. Controlled Fusion*, 49, 447
 Sokoloff, D., Bao, S. D., Kleeorin, N., Kuzanyan, K., Moss, D., Rogachevskii, I., Tomin, D., & Zhang, H. 2006, *Astron. Nachr.*, 327, 876
 van Ballegoijen, A. A., & Martens, P. C. H. 1990, *ApJ*, 361, 283
 van Ballegoijen, A. A., Priest, E. R., & Mackay, D. H. 2000, *ApJ*, 539, 983
 Yang, W. H., Sturrock, P. A., & Antiochos, S. K. 1986, *ApJ*, 309, 383
 Yeates, A. R., Mackay, D. H., & van Ballegoijen, A. A. 2007, *Sol. Phys.*, 245, 87
 ———. 2008, *Sol. Phys.*, 247, 103
 Zhang, M. 2006, *ApJ*, 646, L85
 Zirker, J. B., Martin, S. F., Harvey, K., & Gaizauskas, V. 1997, *Sol. Phys.*, 175, 27